Research Article | Vol. 28, No. 21 / 12 October 2020 / Optics Express 31436

Optics EXPRESS

Influence of micro-structure on modulation properties in VO_2 composite terahertz memory metamaterials

GE LI,[1,2] QINGLI ZHOU,[1,3] CHEN GE,[2,4] WANLIN LIANG,[1] YUWANG DENG,[1] CHANGXIANG LIU,[1] CUNLIN ZHANG,[1] JIANYU DU,[2] AND KUI-JUAN JIN[2]

[1] *Key Laboratory of Terahertz Optoelectronics, Ministry of Education, and Beijing Advanced Innovation Center for Imaging Theory and Technology, Department of Physics, Capital Normal University, Beijing 100048, China*
[2] *Beijing National Laboratory for Condensed Matter Physics Institute of Physics, Chinese Academy of Sciences, Beijing 100190, China*
[3] *qlzhou@cnu.edu.cn*
[4] *gechen@iphy.ac.cn*

Abstract: We have grown VO_2 films and combined with terahertz metamaterials to manipulate the memory effect during the insulator-to-metal transition. The temperature-dependent resonant frequency of hybrid structure shows a thermal hysteresis accompanied with frequency shift and bandwidth variation due to the presence of a VO_2 dielectric layer. This frequency memory effect significantly depends on the metallic micro-structure. Further theoretical calculation demonstrates this phenomenon mainly originates from the different coupling strength between VO_2 and metallic structures. Our findings could facilitate the application of VO_2 films in the smart window and dynamical terahertz modulators.

1. Introduction

Vanadium dioxide (VO_2) has become a focal point of functional oxide research due to its near room-temperature insulator-to-metal phase transition (IMT), resulting from a structural transition around the critical temperature $T_C \approx 340$ K [1–3]. During the IMT process, VO_2 shows a sharp change in resistance and a pronounced optical switching behavior [4–6]. These excellent characteristics make VO_2 material suitable for many promising applications such as smart window, optical switch, and phase transition memory [6–11]. However, its practical applications are greatly limited by the critical temperature and the temperature difference of the hysteresis loop. The ability to manipulate the IMT of VO_2 is of importance for fundamental investigations of electron correlations and practical implementations of power efficient tunable electrical and optical devices [12]. Recently, many efforts have been carried out for the refined IMT modification by chemical doping [13], interfacial strain engineering [14], hydrogenation [15], electrolyte gating [16–18], and light excitation [19]. Consequently, its resistance memory effect can be changed by engineering the material itself. There are few studies about the manipulation of hysteresis loop by metamaterials. This artificial material can achieve unique electromagnetic response, which cannot be obtained in natural materials, such as negative reflection and electromagnetic cloaking [20–23]. Some excellent studies about the metamaterial/VO_2 hybrid devices mainly focus on the dynamical modulation of spectral response, where VO_2 film plays a role as a temperature-dependent dielectric layer [9,24–28]. In addition, Thompson *et al.* [29] reported that the terahertz (THz) nano-antennas can enhance the field-induced phase transition of VO_2 film by intensifying the field strength. This means metamaterials can be used to assist in modulating the resistance memory effect of VO_2. Actually, it is shown that such composite structure combining

#404082 https://doi.org/10.1364/OE.404082
Journal © 2020 Received 30 Jul 2020; revised 24 Sep 2020; accepted 26 Sep 2020; published 5 Oct 2020

Optics EXPRESS

VO_2 with metamaterial could exhibit similar thermal hysteresis phenomenon to acquire frequency memory effect [9,30,31]. Here, we utilized THz metamaterial fabricated on high-quality VO_2 epitaxial film to control the thermal hysteresis loop of the frequency memory curve. Experimental results indicate that the frequency memory effect can be dramatically modulated by using different gold micro-structures. Further theoretical calculations based on the coupled Lorentz oscillator model have been performed, showing that the modulation originates from the influence of the coupling between VO_2 film and metamaterial. This could provide us a pathway to obtain the desired frequency memory device through the flexible design of the metamaterials.

2. Experimental and simulated results

Epitaxial films of VO_2 were prepared on Al_2O_3 substrates from polycrystalline V_2O_5 target by a pulsed laser deposition technique using a laser energy density of ∼1 J/cm^2 and a repetition rate of 4 Hz. The films were grown at 648 K in a flowing oxygen atmosphere with pressure 3.0 Pa and cooled down to room temperature at 20 K/min [18]. In the process of film growth, Al_2O_3 substrates were placed closely on the deposition table to ensure the consistent electrical characteristics of the obtained pure VO_2 films. From the x-ray diffraction pattern of pure VO_2 film before hybrid fabrication with metal structure, we can find only sharp VO_2 $(020)_M$ family peaks emerge without other vanadium oxides in Fig. 1(a) and its zoomed part in Fig. 1(b). Two distinct reflections at $2\theta \sim 39.92°$ and $85.91°$ correspond to the (020) and (040) planes, showing our fabricated VO_2 film is epitaxial with high quality. The temperature-dependent in-plane resistance of the film was measured using the four-probe method, as presented in Fig. 1(c). Around the IMT temperature, the electrical resistance shows an abrupt change with four orders of magnitude. This giant change implies the good electrical property of the VO_2 films. As calculated in the inset, the critical temperatures are determined as 348.8 K and 338.2 K for the warming and cooling processes [32,33], respectively, to achieve the temperature difference ($\Delta T_{diff} = T_{\text{warming}} - T_{\text{cooling}}$) of 10.6 K. Then gold planar arrays (designed as a ring and its split structures, respectively) were fabricated on 50 nm thick VO_2 films by photolithography method. During this process, a layer of photoresist was spin-coated on the film surface, and ultraviolet exposure technology was used to form structure pattern. A 200 nm thick layer of gold (Au) with a 5 nm chrome (Cr) adhesive layer was evaporated on top of the film layer by the magnetron sputtering. The Cr/Au layer was then patterned by the lift-off. Schematic VO_2-metamaterial hybrid structures and the optical images are presented in Fig. 1(d). Our measured temperature-dependent dc resistance curves before and after being patterned with two structures also indicate that the electrical properties of VO_2 films are similar and not affected by the photolithography process with nearly the same critical temperature and hysteresis window (not shown).

It is known that VO_2 undergoes IMT accompanied by an electronic structure variation related to the electronic properties [34]. Since it is sensitive to the carrier density and resistivity, THz wave can be expected to characterize the changes in the internal electronic structure of materials. Here, the temperature dependence of electromagnetic responses was characterized using THz time domain spectroscopy. In this measurement setup, a Spectra Physics regenerative amplifier system produces 800 nm pulses with 100 fs duration and 1 kHz repetition rate. The source beam is split into two portions, corresponding to THz generation and probe beams, respectively. The generation pulse is incident on a <110> ZnTe crystal with thickness of 2 mm to generate THz wave. The transmitted THz wave can be detected by free-space electro-optic sampling in a 1 mm thick <110> ZnTe crystal with the probe pulse [35]. The signal is collected by a lock-in amplifier with phase locked to an optical chopper. The path with THz radiation is enclosed and purged with dry nitrogen. As shown in Fig. 1(d), the THz radiation is normally incident to the sample plane and the electric field $\boldsymbol{E}_{\text{in}}$ is parallel to the x axis. We measured the transmitted THz waves through hybrid structures and utilized the reference signal in free space for comparison to obtain the transmission spectra. Furthermore, the electromagnetic responses of the hybrid

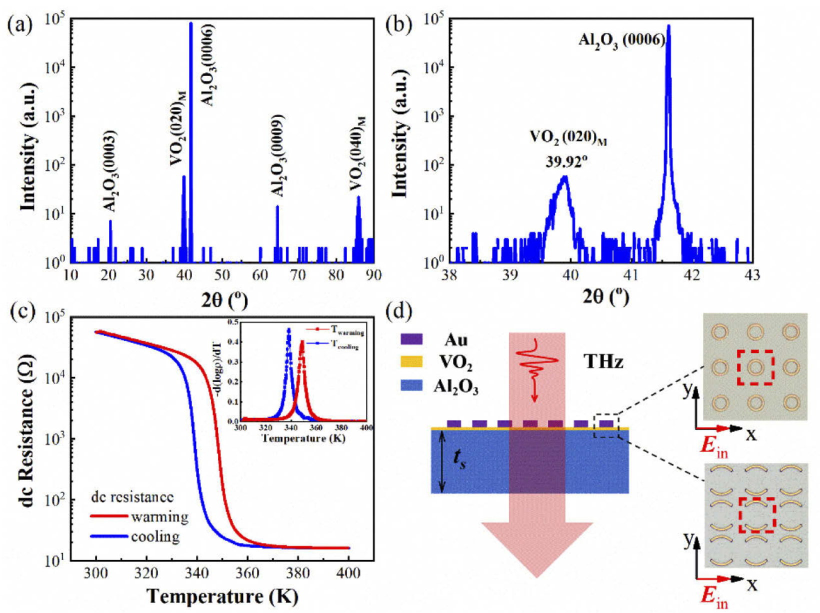

Fig. 1. Symmetrical XRD 2theta-omega scan of VO_2 film ((a) $10° \leq 2\theta \leq 90°$ (b) $38° \leq 2\theta \leq 43°$). (c) Temperature-dependent dc resistance. Inset: temperature derivative of logρ, where ρ is the film resistivity. (d) Schematic VO_2-metamaterial hybrid structures and their optical images. The thickness t_s of Al_2O_3 is 0.5 mm.

structures were simulated by the finite difference time domain method. We construct the model with three layers including Al_2O_3 substrate, VO_2 film layer, and surface metal micro-structure. A unit cell, as shown in Fig. 1(d), was chosen as the simulation domain. The periodic conditions were applied along x and y directions, respectively, and the perfect matched layers were employed along the z direction. The structures were illuminated by the incident wave with the electric field along the x axis. The dielectric constant of Al_2O_3 substrate was set to be 9.6 calculated from our experimental data, and the dielectric constant of VO_2 film was set to be 9 with the conductivity of 10 S/m at room temperature [36]. Au structures were regarded as perfect electric conductors.

Firstly, for our fabricated isotropic single ring structure on the VO_2 film, the outer radius is 13.5 µm with width of 3 µm and the lattice parameter is 60 µm. The simulation result is plotted in Fig. 2(a), showing a sharp resonance dip at 1.64 THz. The insets present the surface current and electric field distributions at this resonant frequency. The in-phase currents appear in the top and bottom arcs, and the electric fields are strongly concentrated in the left and right sides of the single ring structure. The temperature-dependent transmission spectra of this patterned VO_2 sample for warming and cooling processes are measured and depicted in Figs. 2(b) and 2(c), respectively. At room temperature, the resonant frequency located at 1.63 THz shows an agreement with the simulation result. In the warming process, as the dielectric constant of VO_2 film increases with temperature [9], the resonance dip shows red-shift by as much as 17% accompanied with the reduction in resonant absorption and broadening in bandwidth. In the cooling process, as the dielectric constant gradually recovers, the resonant frequency moves back slowly to the initial frequency. Those phenomena could be ascribed to the structural transformation, where the electron density increases abruptly during IMT, leading to a large change in permittivity. The variation in VO_2 film will affect the dielectric environment around the single ring resonator so that the resonant frequency shifts during the IMT process. To further clearly show this effect, we extract the resonant frequencies at different temperatures and compare with the temperature-dependent dc resistance of pure VO_2 film, as shown in Fig. 2(d). Our measured results show the resonant frequency position varies with the temperature. This shift of the resonant frequency in the warming and cooling processes can also form the thermal hysteresis loop, exhibiting the different characteristics from the resistance memory curve in the pure film. It is found that the critical temperature of the resonant frequency slightly moves to high temperature and the temperature difference narrows significantly to 5.4 K.

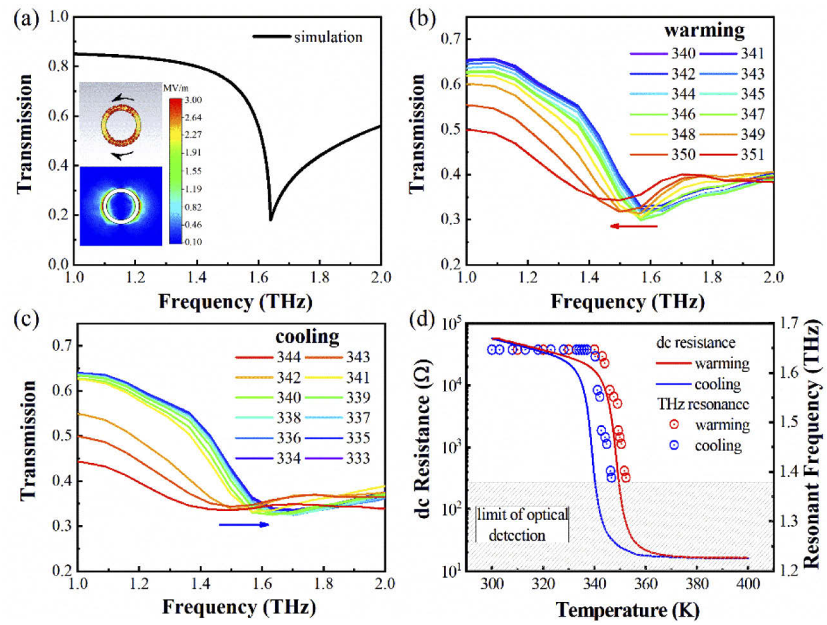

Fig. 2. (a) Simulated transmitted spectrum of the single ring structure. Insets: current and electric field distributions at the resonant frequency, respectively. (b) and (c) are experimental results. (d) Temperature-dependent THz resonant frequency and dc resistance (solid line is temperature-dependent dc resistance of pure VO_2 film).

Then we symmetrically cut the single ring from the center of the ring to destroy the isotropic nature of the structure. In order to make the resonant frequency locate in our studied frequency range, we redesigned the geometrical parameters of the resonator. The outer radius is fixed as 25.5 μm with 3 μm in width, and the width of gap is 37 μm. The simulation results are shown in Fig. 3(a). As the THz electric field is parallel to the gap, a deep resonance appears at 1.52 THz, where the distributions of the current and the electric field are similar to those in the single ring structure. The measured spectral responses in the warming and cooling processes, as shown in Figs. 3(b) and 3(c), respectively, exhibit the same trends with reduction, broadening, and shifts of the resonance dip during the phase transition. In Fig. 3(d), we plot the curve of the resonant frequencies at different temperatures. A significant increase of the critical temperature in the warming process is observed and determined as 356 K, showing 7.2 K and 5.5 K higher than the values for pure VO_2 film and single ring/VO_2 hybrid structure, respectively. Meanwhile, the temperature difference in this frequency memory curve is 10 K, approximate to that of 10.6 K for the grown films, and almost as twice as the value of the single ring structure. From the above results, we could conclude that there is an interactive coupling between the VO_2 film and metamaterial, where VO_2 film gives dielectric nature to metamaterial to realize the dynamical modulation in THz range and the metamaterials with different structures can affect the thermal hysteresis of frequency memory curve to modify the characteristic of VO_2-based metamaterials. Additionally, we have performed the measurement when the incident THz polarization is along the y axis by rotating the split ring sample by 90°. It is observed the transmission spectrum at room temperature is nearly flat without resonant absorption, implying the metal structure has little effect in this direction and the transmission characteristics are mainly determined by the VO_2 film. Our obtained results indicate that we could use the structural anisotropy and polarization sensitivity to obtain the multifunctional characteristics of the THz memory devices.

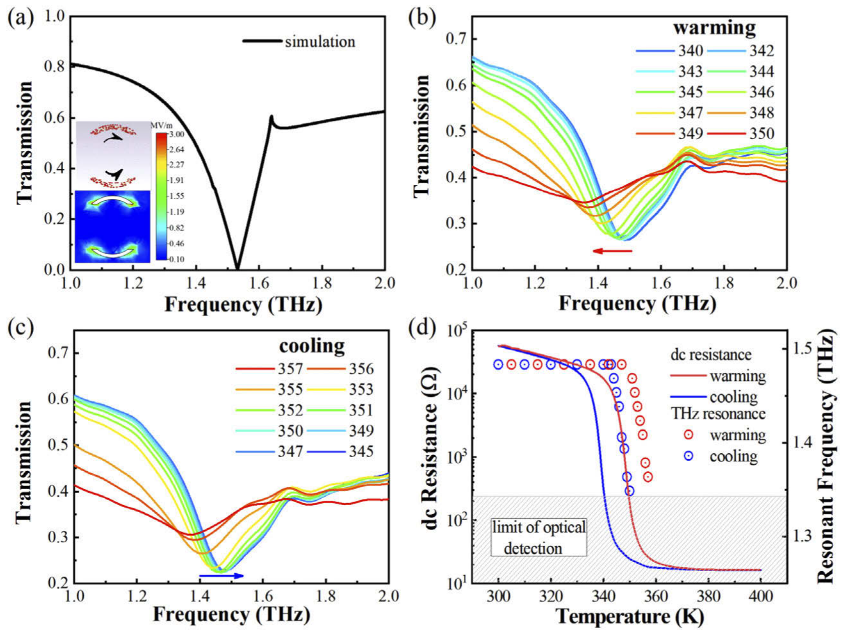

Fig. 3. (a) Simulated transmitted spectrum of the split ring structure. Insets: current and electric field distributions at the resonant frequency, respectively. (b) and (c) are experimental results. (d) Temperature-dependent THz resonant frequency and dc resistance (solid line is temperature-dependent dc resistance of pure VO_2 film).

3. Coupled oscillator theory

To further explain these phenomena and clarify the interaction mechanism between the VO_2 films and metamaterials in THz region, we have performed the analytical calculation based on the coupled Lorentz oscillator theory. The behavior of this coupling model can be described by the following set of equations [37–39]:

$$\ddot{x}_1 + \gamma_1 \dot{x}_1 + \omega_1^2 x_1 + \upsilon_{12} x_2 = a_1 e^{i\omega t}, \tag{1}$$

$$\ddot{x}_2 + \gamma_2 \dot{x}_2 + \omega_2^2 x_2 + \upsilon_{12} x_1 = a_2 e^{i\omega t}, \tag{2}$$

where x_1, x_2, γ_1, γ_2, ω_1, ω_2 are the amplitudes, damping rates and resonant frequencies of the metamaterial and the VO_2 film, respectively. υ_{12} represents the coupling coefficients between their resonances. The geometric parameters a_1 and a_2 indicate the strength of each material coupling to the incident THz field.

Solving the above coupled equations, we can obtain the THz response of metamaterial under the consideration with the coupling of VO_2 film, as shown in Fig. 4 for the single ring and split ring structures, respectively. The THz response intensity of the ring structure at room temperature (black curve) is calculated under the initial values of γ_1=0.025, ω_1=1.63, a_1=2.0, γ_2=0.05, ω_2=1.90, a_2=1.1, and υ_{12}=0.12, as shown in Fig. 4(a). Then with the increasing temperature,

Optics EXPRESS

we chose other two temperatures to perform the theoretical calculation with the parameters of υ_{12}=0.40 and γ_2=0.15 for 344 K (blue curve), and υ_{12}=0.90 and γ_2=0.25 for 351 K (red curve), respectively. It is clear that a red-shift accompanied with the reduction in resonant absorption and broadening in bandwidth can be observed in Fig. 4(a), reflecting the same trend as the measured results. In this warming process, VO_2 undergoes a resistance change to the metallic phase, leading to a stronger coupling effect with the gold structure and a higher absorption of THz wave by VO_2 layer. Hence, the coupling coefficients υ_{12} and the additional damping rate γ_2 introduced by the existence of VO_2 films will increase correspondingly. Here, the calculated response intensity to external THz field could represent the resonant absorption of the sample. The decreased THz response intensity leads to the reduction in absorption and enhancement in transmission, showing being consistent with the experimental observation with dashed lines. It is worth noting that our theoretical calculated curve is the THz response of the metamaterial structure under the coupling effect introduced by the VO_2 film. However, the transmission observed experimentally is the response of the whole sample involving the metamaterial and the film. Although the resonant response intensity of the metamaterial decreases with the increased temperature to enhance the transmission, the film conductivity increases on the contrary to reduce the transmission through the absorption of THz wave. Therefore, the experimental transmission change with the temperature is less obvious compared with the change of calculated THz response intensity of the metamaterial.

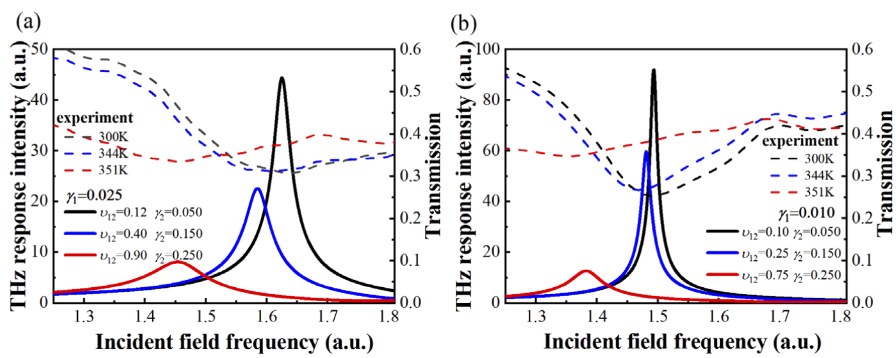

Fig. 4. Calculated THz response intensities of VO_2 hybrid structure under the different damping rate γ_2 and coupling coefficient υ_{12} for (a) single ring structure and (b) split ring structure, respectively. The dashed lines are the corresponding experimental data at the different temperature. (black curves: room temperature, blue curves: 344 K, red curves: 351 K.)

Then, we have carried out the theoretical calculation on the split ring structure, as given in Fig. 4(b). The THz response intensity is calculated under the initial values of γ_1=0.01, ω_1=1.50, a_1=1.5, and υ_{12}=0.10 with the identical parameters of γ_2, ω_2, and a_2 for VO_2 at room temperature. As the temperature is increased with the increasing υ_{12} and γ_2, the spectral evolution is similar to the experimental curve. Compared with the single ring structure, parameter selection in this structure has a smaller γ_1 due to its narrower full width of half maximum. Besides, the geometric parameter a_1 varies as well, suggesting different metallic structure has different response strength to the external incident THz field. It should be noticed that at the same temperature the coupling coefficient υ_{12} of VO_2 and metamaterial in the single ring structure is larger than that in the split ring structure, implying stronger coupling effect and larger frequency shift in the former. For the single ring structure, the values of frequency shift are 0.040 from room temperature to 344 K and 0.131 from 344 K to 351 K, respectively. However, for the split ring structure, the corresponding values are 0.013 and 0.099, respectively, due to the smaller υ_{12}.

Optics EXPRESS

The frequency shift in former is larger than that in the latter, indicating the single ring structure has a lower critical temperature in temperature-dependent resonant frequency memory curve, which is consistent with the experimental results. On the other hand, the split ring structure needs to reach a higher temperature to obtain the same frequency shift, leading to a higher transition temperature. Similarly, because the latter is less sensitive to the temperature change, the frequency shift recovery is slower in the cooling process to form the thermal hysteresis loop with a wider window width. Meanwhile, the unchanged value of parameter γ_2 for VO_2 film at specific temperature has been proved by the temperature-dependent dc resistance measurement before and after being patterned with these two structures, showing the resistance thermal hysteresis loops are almost the same.

Additionally, the influence of the coupling and damping of VO_2 with metamaterials has been theoretically studied by modulating the parameters υ_{12} and γ_2 as shown in Fig. 5, while keeping other parameters unchanged. For the single ring structure in Fig. 5(a), it can be seen that υ_{12} determines frequency shift and intensity of THz response, showing the exponential growth in red-shift and off-resonant regions with the increased coupling, while the THz intensity in resonant region is exponential decay with υ_{12}. For the split ring structure in Fig. 5(b), we observe the similar characteristics and trend, only different in the variation range of red-shift and response intensity. Damping rate γ_2 as an important parameter mainly affects the shape as well as the bandwidth of the resonance. Figure 5(c) shows an exponential increasing of bandwidth with γ_2 of these two hybrid structures. Resonance bandwidth curves indicate that the single ring structure has a greater broadening as γ_2 increases. These are consistent with our experimental measurements and the observed spectral evolution with the temperature. Through above theoretical calculation, we can find the spectral response of the designed hybrid structure

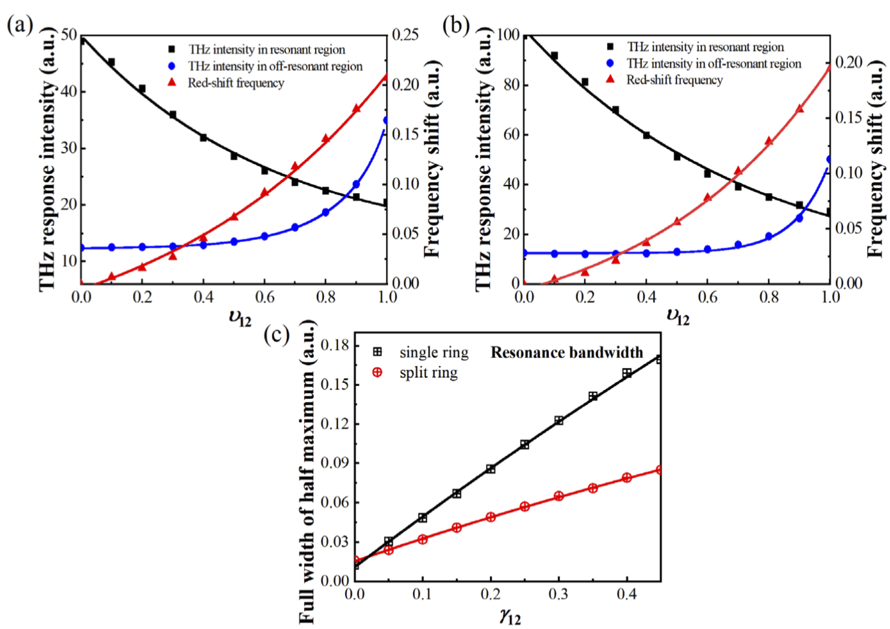

Fig. 5. Influence of υ_{12} on THz intensity in resonant region (black squares), off-resonant region (blue dots) and frequency red-shift (red triangles) for (a) single ring structure and (b) split ring structure, respectively. The curves are the exponential fitting. (c) Dependency between bandwidth and γ_2 of these two hybrid structures. The curves are the exponential fitting.

during the IMT process can be well described by this coupled oscillator theory to further help us to understand the internal coupling mechanism of the VO_2/metamaterial structure.

Based on this work, we could develop a strategy combined with the phase transition film and different metamaterial structure to manipulate and realize our expected frequency memory effect through the coupling in hybrid structure. Due to the significant dependence on the metal micro-structure, we could firstly design and simulate the composite structures to obtain their spectral properties, and then carry out the theoretical calculation with the coupling model to acquire the coupling and damping coefficients. Through the analysis of the coupling change with the temperature, the frequency shift and spectral line shape of the composite structures are predicted theoretically to extract the frequency memory curve, which can also be proved by the simulation. According to the actual demand, the specific hybrid structure can be chosen to fabricate and apply in the THz optoelectronic components.

4. Conclusion

In summary, we have grown high quality VO_2 films confirmed by the x-ray diffraction. The studies on VO_2 composite THz metamaterials demonstrate that the isotropic/anisotropic metamaterial structures affect the critical temperature and temperature difference of the frequency memory curve of the hybrid structures greatly due to their different coupling behavior between VO_2 film and metallic structure. Theoretical calculation based on a coupling model is employed to reveal this coupling in THz region. Calculation results agree well with experimental results, and further prove the coupling coefficient and damping rate have a significant impact on the spectral evolution. Our work provides an effective method to realize the frequency memory effect and advances the understanding of the interactions between the VO_2 films and metamaterials. Such kind of hybrid structures will open the door for high-performance VO_2-based smart window application and expand potential applications in dynamical THz modulators and phase transition memory devices.

Funding

Youth Innovation Promotion Association of the Chinese Academy of Sciences (2018008); Natural Science Foundation of Beijing Municipality (4181001); National Key Research and Development Program of China (2017YFA0303604); National Natural Science Foundation of China (11574219, 11674385, 61875140).

Acknowledgments

The authors are thankful to Dr. Jian Zuo and Zihan Zhou for insightful discussion and help in sample measurement.

Disclosures

The authors declare no conflicts of interest.

References

1. M. M. Qazilbash, M. Brehm, B. G. Chae, P. C. Ho, G. O. Andreev, B. J. Kim, S. Y. Yun, A. V. Balatsky, M. B. Maple, F. Keilmann, H. T. Kim, and D. N. Basov, "Mott transition in VO_2 revealed by infrared spectroscopy and Nano-imaging," Science **318**(5857), 1750–1753 (2007).
2. N. B. Aetukuri, A. X. Gray, M. Drouard, M. Cossale, L. Gao, A. H. Reid, R. Kukreja, H. Ohldag, C. A. Jenkins, E. Arenholz, K. P. Roche, H. A. Durr, M. G. Samant, and S. S. P. Parkin, "Control of the metal–insulator transition in vanadium dioxide by modifying orbital occupancy," Nat. Phys. **9**(10), 661–666 (2013).
3. Q. Y. Lu, S. R. Bishop, D. Lee, S. Lee, H. Bluhm, H. L. Tuller, H. N. Lee, and B. Yildiz, "Electrochemically triggered metal–insulator transition between VO_2 and V_2O_5," Adv. Funct. Mater. **28**(34), 1803024 (2018).

4. S. Chen, X. J. Wang, L. L. Fan, G. M. Liao, Y. L. Chen, W. S. Chu, L. Song, J. Jiang, and C. W. Zou, "The dynamic phase transition modulation of ion-liquid gating VO_2 thin film: formation, diffusion, and recovery of oxygen vacancies," Adv. Funct. Mater. **26**(20), 3532–3541 (2016).
5. K. Abbas, J. Hwang, G. Bae, H. Choi, and D. J. Kang, "Control of multilevel resistance in vanadium dioxide by electric field using hybrid dielectrics," ACS Appl. Mater. Interfaces **9**(15), 13571–13576 (2017).
6. S. Chen, Z. W. Wang, H. Ren, Y. L. Chen, W. S. Yan, C. M. Wang, B. W. Li, J. Jiang, and C. W. Zou, "Gate-controlled VO_2 phase transition for high-performance smart windows," Sci. Adv. **5**(3), eaav6815 (2019).
7. H. Kim, Y. Kim, K. S. Kim, H. Y. Jeong, A. R. Jang, S. H. Han, D. H. Yoon, K. S. Suh, H. S. Shin, T. Kim, and W. S. Yang, "Flexible thermochromic window based on hybridized VO_2/Graphene," ACS Nano **7**(7), 5769–5776 (2013).
8. T. Wang, D. Torres, F. E. Fernández, A. J. Green, C. Wang, N. Sepùlveda, N. Wang, T. Torres, D. Fernández, F. E. B. Green, A. J. C. Wang, and C. A. Sepùlveda, "Increasing efficiency, speed, and responsivity of vanadium dioxide based photothermally driven actuators using single-wall carbon nanotube thin-films," ACS Nano **9**(4), 4371–4378 (2015).
9. T. Driscoll, H. T. Kim, B. G. Chae, B. J. Kim, Y. W. Lee, N. M. Jokerst, S. Palit, D. R. Smith, M. D. Ventra, and D. N. Basov, "Memory metamaterials," Science **325**(5947), 1518–1521 (2009).
10. H. Zhu, L. Du, J. Li, Q. Shi, B. Peng, Z. Li, W. Huang, and L. Zhu, "Near-perfect terahertz wave amplitude modulation enabled by impedance matching in VO_2 thin films," Appl. Phys. Lett. **112**(8), 081103 (2018).
11. S. Chen, H. Yuan, Z. Zhai, L. Du, S. Zhong, H. Zhu, Q. Shi, W. Huang, Z. Li, and L. Zhu, "All optically driven memory device for terahertz waves," Opt. Lett. **45**(1), 236–239 (2020).
12. Q. Jia, J. Grenzer, H. B. He, W. Anwand, Y. D. Ji, Y. Yuan, K. Huang, T. G. You, W. J. Yu, W. Ren, X. Z. Chen, M. K. Liu, S. Facsko, X. Wang, and X. Ou, "3D local manipulation of the metal–insulator transition behavior in VO_2 thin film by defect-induced lattice engineering," Adv. Mater. Interfaces **5**(8), 1701268 (2018).
13. J. G. Ramirez, T. Saerbeck, S. Wang, J. Trastoy, M. Malnou, J. Lesueur, J. P. Crocombette, J. E. Villegas, and I. K. Schuller, "Effect of disorder on the metal-insulator transition of vanadium oxides: local versus global effects," Phys. Rev. B **91**(20), 205123 (2015).
14. L. Fan, S. Chen, Z. Luo, Q. Liu, Y. Wu, L. Song, D. Ji, P. Wang, W. Chu, and C. Gao, "Strain dynamics of ultrathin VO_2 film grown on TiO_2 (001) and the associated phase transition modulation," Nano Lett. **14**(7), 4036–4043 (2014).
15. H. Yoon, M. Choi, T. W. Lim, H. Kwon, K. Ihm, J. K. Kim, S. Y. Choi, and J. Son, "Reversible phase modulation and hydrogen storage in multivalent VO_2 epitaxial thin films," Nat. Mater. **15**(10), 1113–1119 (2016).
16. J. del Valle, P. Salev, F. Tesler, N. M. Vargas, Y. Kalcheim, P. Wang, J. Trastoy, M. Lee, G. Kassabian, J. G. ramírez, M. J. rozenberg, and I. K. Schuller, "Subthreshold firing in Mott nanodevices," Nature **569**(7756), 388–392 (2019).
17. J. Jeong, N. Aetukuri, T. Graf, T. D. Schladt, M. G. Samant, and S. S. P. Parkin, "Suppression of metal-insulator transition in VO_2 by electric field–induced oxygen vacancy formation," Science **339**(6126), 1402–1405 (2013).
18. C. Ge, G. Li, Q. L. Zhou, J. Y. Du, E. J. Guo, M. He, C. Wang, G. Z. Yang, and K. J. Jin, "Gating-induced reversible H_xVO_2 phase transformations for neuromorphic computing," Nano Energy **67**, 104268 (2020).
19. H. T. Zhang, L. Guo, G. Stone, L. Zhang, Y. X. Zheng, E. Freeman, D. W. Keefer, S. Chaudhuri, H. Paik, and J. A. Moyer, "Imprinting of local metallic states into VO_2 with ultraviolet light," Adv. Funct. Mater. **26**(36), 6612–6618 (2016).
20. D. R. Smith, W. J. Padilla, D. C. Vier, S. C. Nemat-Nasser, and S. Schultz, "Composite medium with simultaneously negative permeability and permittivity," Phys. Rev. Lett. **84**(18), 4184–4187 (2000).
21. R. A. Shelby, D. R. Smith, and S. Schultz, "Experimental verification of a negative index of refraction," Science **292**(5514), 77–79 (2001).
22. W. J. Padilla, A. J. Taylor, C. Highstrete, M. Lee, and R. D. Averitt, "Dynamical electric and magnetic metamaterial response at terahertz frequencies," Phys. Rev. Lett. **96**(10), 107401 (2006).
23. H. T. Chen, W. J. Padilla, J. M. O. Zide, A. C. Gossard, A. J. Taylor, and R. D. Averitt, "Active terahertz metamaterial devices," Nature **444**(7119), 597–600 (2006).
24. M. Liu, H. Y. Hwang, H. Tao, A. C. Strikwerda, K. Fan, G. R. Keiser, A. J. Sternbach, K. G. West, S. Kittiwatanakul, J. Lu, S. A. Wolf, F. G. Omenetto, X. Zhang, K. A. Nelson, and R. D. Averitt, "Terahertz-field-induced insulator-to-metal transition in vanadium dioxide metamaterial," Nature **487**(7407), 345–348 (2012).
25. G. Zhou, P. Dai, J. Wu, B. Jin, Q. Wen, G. Zhu, Z. Shen, C. Zhang, L. Kang, W. Xu, J. Chen, and P. Wu, "Broadband and high modulation-depth THz modulator using low bias controlled VO_2- integrated metasurface," Opt. Express **25**(15), 17322–17328 (2017).
26. C. Zhang, G. Zhou, J. Wu, Y. Tang, Q. Wen, S. Li, J. Han, B. Jin, J. Chen, and P. Wu, "Active Control of terahertz waves using vanadium-dioxide-embedded metamaterials," Phys. Rev. Appl. **11**(5), 054016 (2019).
27. F. Hu, H. Wang, X. Zhang, X. Xu, W. Jiang, Q. Rong, S. Zhao, M. Jiang, W. Zhang, and J. Han, "Electrically triggered tunable terahertz band-pass filter based on VO_2 hybrid metamaterial," IEEE J. Sel. Top. Quantum Electron. **25**(3), 4700207 (2019).
28. Y. Jeong, Y. Bahk, and D. Kim, "Dynamic terahertz plasmonics enabled by phase-change materials," Adv. Opt. Mater. **8**(3), 1900548 (2020).
29. Z. J. Thompson, A. Stickel, Y. Jeong, S. Han, B. H. Son, M. J. Paul, B. Lee, A. Mousavian, G. Seo, H. Kim, Y. Lee, and D. Kim, "Terahertz-triggered phase transition and hysteresis narrowing in a nanoantenna patterned vanadium dioxide film," Nano Lett. **15**(9), 5893–5898 (2015).

30. M. Seo, J. Kyoung, H. Park, S. Koo, H. Kim, H. Bernien, B. J. Kim, J. H. Choe, Y. H. Ahn, H. Kim, N. Park, Q. Park, K. Ahn, and D. Kim, "Active terahertz nanoantennas based on VO_2 phase transition," Nano Lett. **10**(6), 2064–2068 (2010).
31. H. Liu, J. Lu, and X. R. Wang, "Metamaterials based on the phase transition of VO_2," Nanotechnology **29**(2), 024002 (2018).
32. J. H. Shin, K. Moon, E. S. Lee, I. M. Lee, and K. H. Park, "Metal-VO_2 hybrid grating structure for a terahertz active switchable linear polarizer," Nanotechnology **26**(31), 315203 (2015).
33. C. H. Chen, Y. H. Zhu, Y. Zhao, J. H. Lee, H. Y. Wang, A. Bernussi, M. Holtz, and Z. Y. Fan, "VO_2 multidomain heteroepitaxial growth and terahertz transmission modulation," Appl. Phys. Lett. **97**(21), 211905 (2010).
34. S. Chen, Z. W. Wang, L. L. Fan, Y. L. Chen, H. Ren, H. Ji, D. Natelson, Y. Y. Huang, J. Jiang, and C. W. Zou, "Sequential insulator-metal-insulator phase transitions of VO_2 triggered by hydrogen doping," Phys. Rev. B **96**(12), 125130 (2017).
35. Q. Wu, M. Litz, and X. C. Zhang, "Broadband detection capability of ZnTe electro-optic field detectors," Appl. Phys. Lett. **68**(21), 2924–2926 (1996).
36. F. Fan, Y. Hou, Z. W. Jiang, X. H. Wang, and S. J. Chang, "Terahertz modulator based on insulator-metal transition in photonic crystal waveguide," Appl. Opt. **51**(20), 4589–4596 (2012).
37. X. Su, C. Ouyang, N. Xu, S. Tan, J. Gu, Z. Tian, R. Singh, S. Zhang, F. Yan, J. Han, and W. Zhang, "Dynamic mode coupling in terahertz metamaterials," Sci. Rep. **5**(1), 10823 (2015).
38. Q. Wang, Y. Huang, Z. Yao, and X. Xu, "Analysis of transition from Lorentz resonance to Fano resonance in plasmon and metamaterial systems," Opt. Quantum Electron. **48**(2), 83 (2016).
39. J. Li, Y. Zhou, B. Quan, X. Pan, X. Xu, Z. Ren, F. Hu, H. Fan, M. Qi, J. Bai, L. Wang, J. Li, and C. Gu, "Graphene–metamaterial hybridization for enhanced terahertz response," Carbon **78**, 102–112 (2014).